Appl. Phys. B 78, 503–511 (2004)
DOI: 10.1007/s00340-003-1380-7

**Applied Physics B**
**Lasers and Optics**

J.T.C. LIU✉
J.B. JEFFRIES
R.K. HANSON

# Wavelength modulation absorption spectroscopy with 2*f* detection using multiplexed diode lasers for rapid temperature measurements in gaseous flows

High Temperature Gasdynamics Laboratory, Department of Mechanical Engineering, Stanford University, Stanford, CA 94305, USA

**Received: 7 August 2003/Revised version: 31 October 2003**
**Published online: 5 February 2004 •** 

**ABSTRACT** Multiplexed fiber-coupled diode lasers are used to probe second-harmonic line shapes of two near-infrared water absorption features, at 1343 nm and 1392 nm, in order to infer temperatures in gases containing water vapor, such as combustion flows. Wavelength modulation is performed at 170 kHz, and is superimposed on 1-kHz wavelength scans in order to recover full second-harmonic line shapes. Digital waveform generation and lock-in detection are performed using a data-acquisition card installed in a PC. An optimal selection of the modulation indices is shown to greatly simplify data interpretation over extended temperature ranges and to minimize the need for calibration when performing 2*f* ratio thermometry. A theoretical discussion of this optimized strategy for 2*f* ratio thermometry, as well as results from experimental validations in a heated cell, at pressures up to atmospheric, are presented in order to illustrate the utility of this technique for rapid temperature measurements in gaseous flow fields.

**PACS** 42.62.Fi; 42.55.Px; 42.60.Fc; 39.30.+w

## 1 Introduction

Diode laser absorption-based sensors have been researched extensively as a method for making sensitive and fast (kilohertz bandwidth) in situ measurements in combustion environments, as well as for other gaseous or plasma applications such as semiconductor processing [1–8]. Diode lasers have been used to infer species concentrations, pressures, temperatures, and velocities by rapidly scanning laser radiation across isolated absorption features and recording highly resolved absorption line shapes. The use of wavelength-multiplexed diode lasers has shown great advantages for making temperature measurements in hot gases by line-ratio thermometry [2, 3, 8–10]. In ratio thermometry, multiple diode lasers are used to simultaneously scan across isolated absorption features, or a single laser is used to scan across adjacent absorption features [4] with line strengths that exhibit different temperature dependences due to differences in the lower-state energies of the chosen absorption transitions. By taking ratios of peak absorbance or ratios of spectrally integrated absorbance (line strength), temperature is inferred while eliminating the need to know species concentrations [11]. A plot of line strength versus temperature for the two water features employed in this study is shown in Fig. 1.

In continuous diode laser measurements, drifts in laser intensities over time occur due to thermal, mechanical, and electronic effects. Therefore, scanned wavelength methods are beneficial because the non-absorbing wings of the spectroscopic features may be used to infer a zero-absorption intensity baseline with each laser scan (usually at kilohertz rates or higher). This assumes that the pressures are low enough, and the absorption lines sufficiently well selected, such that the features of interest are spectrally isolated from neighboring features. For direct absorption measurements with diode lasers, the polynomial fit generally employed to determine the zero-absorption baseline is a critical step in extracting accurate line shapes [12]. Low signal levels and/or various noise sources such as baseline-fitting errors, turbulent flow field-induced beam steering, fiber mode distortion, and etalon effects, often hamper the accurate determination of line shapes.

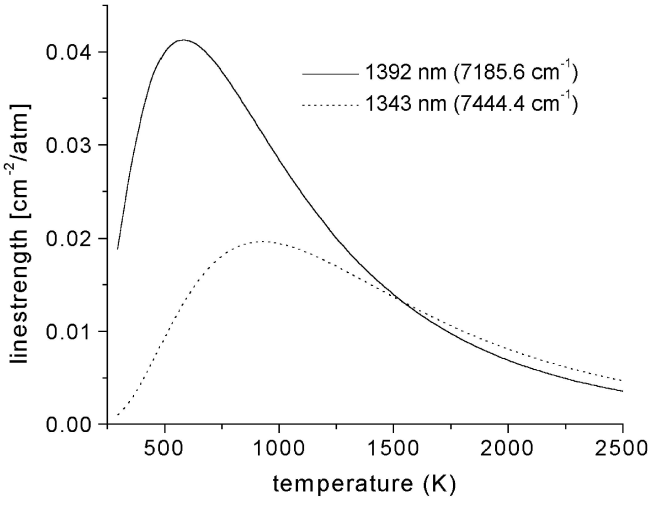


**FIGURE 1** Simulated line strengths versus temperature (HITEMP database [25])

✉ Fax: +1-650/723-1748, E-mail: jonliu@stanford.edu

Wavelength modulation, in conjunction with second-harmonic ($2f$) detection, is well known as a means to increase signal to noise ratios (SNRs) but at the expense of ease of interpretation and simplicity of design [4, 14]. However, for temperature measurements, taking $2f$ peak ratios of absorption features, and making a judicious choice of modulation indices, will be shown to simplify signal interpretation and reduce the need for calibration over large temperature ranges. Also, with the advent of modern computer technologies and software, it is possible to perform wavelength modulation spectroscopy (WMS) using digital waveform generation and lock-in detection at hundred-kilohertz rates without dedicated signal generation or lock-in hardware [15]. Commercial digital lock-ins are available, but generally do not offer the multi-channel capabilities and customization that software lock-ins provide on a PC.

For certain combustion environments, $2f$ spectroscopy is a simple method of yielding temperature measurements with higher accuracy and bandwidth than direct absorption measurements alone [4]. For example, the baseline fitting that is required to extract absorption line shapes in scanned direct absorption measurements is a large source of uncertainty and error that can be effectively eliminated with $2f$ strategies. Baseline fitting is especially problematic in the case of weak absorption features, for which it is difficult to determine where a zero-absorption baseline begins and ends. At elevated pressures, absorption features often combine and broaden to such an extent that the determination of a laser intensity zero-absorption baseline is not possible, especially when transmission fluctuations occur due to beam steering from thermal gradients or mechanical vibrations. In addition, small changes in the fitted baseline can significantly alter the apparent line strength and shape of a feature. Second-harmonic line shapes improve SNR as well as reduce the sensitivity to baseline-fitting errors, since they are sensitive to line-shape curvature, making them advantageous in dealing with noisy signals and weak absorption features.

Various attempts have been made to extract quantitative temperature and species information in combustion gases using modulation techniques. These reports all corroborate the potential of modulation methods for gas sensing, and provide a comparison of different implementations of modulation spectroscopy such as low-frequency WMS with $2f$ line-shape fitting [16], two-tone FM spectroscopy [17], and modulation-frequency-based multiplexing of lasers [18]. It is important to note that various implementations of $2f$ peak ratio thermometry using WMS have already been performed [4, 16, 18], including the use of a single laser to probe two adjacent oxygen transitions [4] and the use of a slow-scanning external cavity diode laser (ECDL) to scan OH transitions in a flame [16]. In the latter case, temperatures were inferred with large uncertainties through least-square fits of $2f$ line shapes in order to iterate upon an initially assumed temperature. In this paper, we present a straightforward method of performing and interpreting $2f$ ratios for rapid temperature measurements by using fast-scanning digital electronics and by optimizing modulation indices. In addition to a theoretical discussion of $2f$ peak ratio optimization for temperature measurements, experimental validations of the theory are shown. The optimal selection of modulation indices allows one to relate $2f$ peak ratios directly to line-strength ratios over large temperature ranges, thereby minimizing the need for calibration. This is a concept that, to our knowledge, has not been explored previously in the literature.

## 2 Wavelength modulation spectroscopy

### 2.1 *Overview*

There is much in the literature about wavelength modulation spectroscopy and $2f$ line shapes, as well as experimental validations of the theory [19–21]. Some of the basic theory will be presented here, in order to explain certain experimental choices made in this study. The discussion will follow the work of Reid and Labrie [20] as well as the extension to account for amplitude modulation covered by Philippe and Hanson [21]. A more rigorous derivation, which is consistent with the presentation below, has been performed by Kluczynski and Axner [22].

Assuming that a sinusoidal modulation is riding on a constant dc diode laser injection current (or a slowly varying ramp, in relation to the sinusoidal modulation frequency), the instantaneous laser frequency, $\nu(t)$, and output intensity, $I_0(t)$, may respectively be expressed as

$$\nu(t) = \bar{\nu} + a\cos(\omega t), \tag{1}$$

$$I_0(t) = \bar{I}_0 + i_0\cos(\omega t + \psi). \tag{2}$$

The modulation frequency is given by $\omega$, $\psi$ is the phase shift between the intensity modulation and the wavelength modulation, while $a$ and $i_0$ are the amplitudes of modulation around $\bar{\nu}$ and $\bar{I}_0$, which are the slowly varying values of the average wavelength and injection current. Laser intensity and wavelength are assumed to vary linearly with injection current in this analysis, which is an appropriate assumption for the hardware and modulation parameters employed here.

The Beer–Lambert relation gives the transmitted intensity, $I_\mathrm{t}$, of monochromatic radiation after passing through an absorbing gas, here given for a uniform gas medium:

$$\tau(\nu) = \left(\frac{I_\mathrm{t}}{I_0}\right)_\nu = \mathrm{e}^{-\alpha(\nu)L}. \tag{3}$$

Here $\tau(\nu)$ is the transmission coefficient, $I_0$ is the incident radiation intensity, $\alpha(\nu)$ is the absorption coefficient, and $L$ is the optical absorbing path length. The absorption coefficient is the product of line strength, $S\,[\mathrm{cm}^{-2}/\mathrm{atm}]$, absorbing species partial pressure, $p_i$ [atm], and line-shape function $\varphi(\nu)$ [cm] : $\alpha(\nu) = S\varphi(\nu)p_i$.

The transmission coefficient, $\tau(\nu) = \tau(\bar{\nu} + a\cos(\omega t))$, is a periodic even function in $\omega t$, and can be expanded in a Fourier cosine series,

$$\tau(\bar{\nu} + a\cos(\omega t)) = \sum_{k=0}^{\infty} H_k(\bar{\nu}, a)\cos(k\,\omega t), \tag{4}$$

where the functions $H_k(\bar{\nu})$ are given as

$$H_0(\bar{\nu}, a) = \frac{1}{2\pi}\int_{-\pi}^{+\pi} \tau(\bar{\nu} + a\cos\theta)\mathrm{d}\theta, \tag{5}$$

$$H_k(\bar{\nu}, a) = \frac{1}{\pi}\int_{-\pi}^{+\pi} \tau(\bar{\nu} + a\cos\theta)\cos k\,\theta\,\mathrm{d}\theta. \tag{6}$$

For $2f$ detection, a lock-in amplifier is used to isolate the second-harmonic signal. The remaining signal, which contains the second-harmonic component of the Fourier sum in (4), is given by the relation

$$S_2(\bar{\nu}) = \frac{i_0}{2}H_3(\bar{\nu}, a) + \bar{I}_0 H_2(\bar{\nu}, a) + \frac{i_0}{2}H_1(\bar{\nu}, a). \tag{7}$$

Here we assume that the phase shift between the laser intensity modulation and the optical frequency modulation is negligible. In addition, we have ignored the effects of nonlinearities in the modulation, which create harmonic distortions that are manifested as a background $2f$ signal. These residual amplitude modulation (RAM) effects are discussed in detail by Kluczynski and Axner [22] but are not significant at the lower modulation depths employed in this study.

For optically thin samples, $\alpha(\nu)L << 1$ (or less than about 0.10), the transmission coefficient reduces to

$$\tau = \exp(-\alpha L) \approx 1 - \alpha L = 1 - S\varphi p_i L \tag{8}$$

and the second-harmonic Fourier component simplifies [13] as

$$H_2(\bar{\nu}, a) = -\frac{Sp_iL}{\pi}\int_{-\pi}^{+\pi} \varphi(\bar{\nu} + a\cos\theta)\cos 2\,\theta\,\mathrm{d}\theta. \tag{9}$$

Therefore, the $2f$ peak height is only complicated by the lineshape function, $\varphi$. In order to infer gas temperature by taking ratios of $2f$ peak heights, it is desired that the ratios should only depend upon the well-known line strengths, $S$, of the selected absorption features. This is possible if the integral in (9) is either constant or varies similarly with respect to temperature for each absorption feature, since $p_i$ and $L$ cancel in the ratios. This requires wisdom in choosing the modulation index, $m$, which is defined as

$$m = \frac{a}{\Delta\nu}, \tag{10}$$

where $\Delta\nu$ is the half width at half maximum (HWHM) of the absorption line. Figure 2 illustrates how the line-center $2f$ peak height varies as a function of $m$ for Gaussian (Doppler-broadened) and Lorentzian (pressure-broadened) line shapes. The functionality is due entirely to the integral in (9). The peak value occurs at $m \sim 2.2$ for all line shapes, as shown by Reid and Labrie [20]. The second-harmonic signal strength that is simulated in Fig. 2 is calculated by numerically integrating (9) for Gaussian line shapes. For Lorentzian line shapes, an exact solution to the integral in (9) is used to calculate signal strengths [23].

While the second Fourier component, $H_2$, is the dominant term in (7), the effects of amplitude modulation are introduced through the higher-order terms containing $i_0$. These terms introduce asymmetries into the $2f$ line shapes. However, since $H_1$ and $H_3$ are odd functions that are zero-valued at peak center in the case of isolated and symmetric absorption features, the line-center $2f$ peak height is unaffected by the presence of amplitude modulation distortions. For this reason, measuring line-center $2f$ peak heights offers a simplifying advantage over measuring other parameters such as peak-to-trough amplitudes or full $2f$ line shapes. Figure 3 shows simulations of the various terms that contribute to the measured $2f$ signal, $S_2$, in (7). For this simulation, $m \sim 2.2$ and the intensity modulation depth was assumed to be 15% ($i_0 = 0.15\bar{I}_0$), which was typical for the lasers and experimental conditions utilized in this work. The relative magnitudes of the higher-order terms in (7) are depicted in this plot, along with the measured $2f$ line shape, which is the sum of the terms. The simulations clearly illustrate that laser inten-

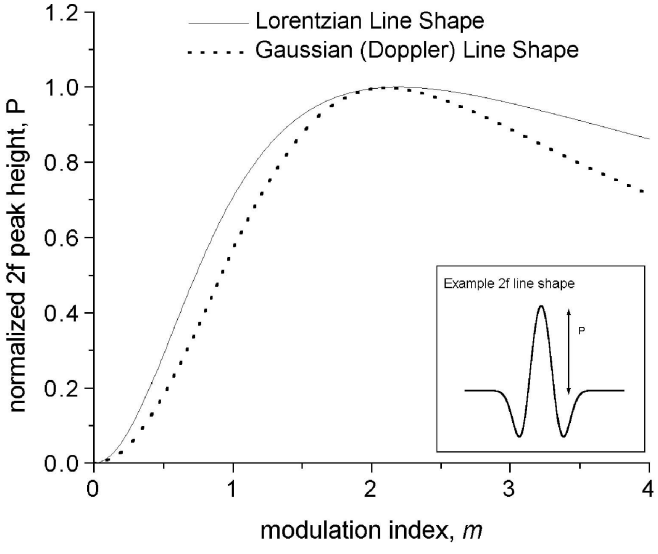


**FIGURE 2** Normalized $2f$ peak height versus $m$ for a Lorentzian and a Gaussian line shape

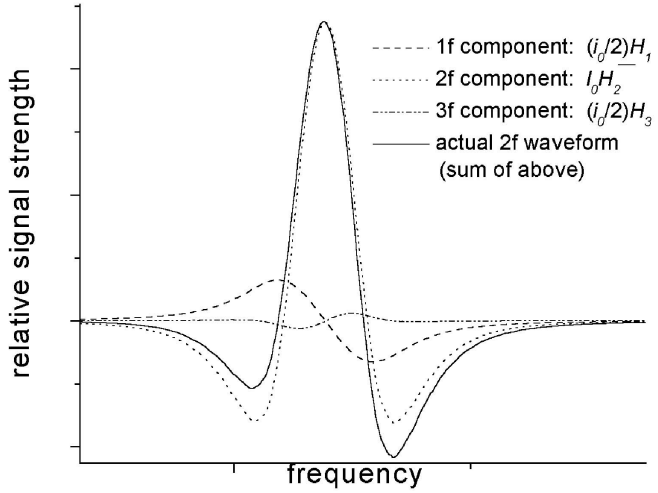


**FIGURE 3** Harmonic components to the $2f$ signal due to laser intensity modulation effects (7). $m \sim 2.2$; $i_0 = 0.15\bar{I}_0$

sity modulation effects do not alter the line-center $2f$ peak heights.

### 2.2 *Optimization*

Temperature measurements using $2f$ spectroscopy are complicated by the fact that the modulation index, $m$, varies with temperature through $\Delta\nu$ in (10). Doppler (Gaussian) line widths vary with the square root of $T$ whereas collisional (Lorentzian) widths vary with $T$ according to an inverse power law:

$$\Delta\nu_{\mathrm{D}} = 3.581\times10^{-7}\nu_0\sqrt{T/M}, \tag{11}$$

$$\Delta\nu_{\mathrm{L}} = P\sum_j \chi_j\gamma_j^{T_0}\left(\frac{T_0}{T}\right)^{n_j}. \tag{12}$$

In (11) and (12), $\Delta\nu_{\mathrm{D}}$ and $\Delta\nu_{\mathrm{L}}$ are the Doppler and Lorentzian half widths at half maximum (HWHM), respectively, in wavenumber ($\mathrm{cm}^{-1}$) units. $\nu_0$ is the line-center position of the feature in $\mathrm{cm}^{-1}$, $T$ is the temperature in Kelvin, and $M$ is the atomic mass (a.m.u.). $P$ is the total pressure in atmospheres, $\chi_j$ is the mole fraction of the $j$th component of the gas mixture, $\gamma_j^{T_0}$ is the pressure-broadening coefficient (half width) at reference temperature $T_0$ for the $j$th perturbing species ($\mathrm{cm}^{-1}/\mathrm{atm}$), and $n_j$ is the species-dependent temperature coefficient.

For Doppler-broadened line shapes, the line-shape function, $\varphi$, only varies with temperature and is nearly identical for all absorption features probed by a multiplexed beam (assuming similar values of $\nu_0$). Therefore, choosing identical modulation indices, $m$, for each absorption feature insures that the integral in (9) cancels when taking $2f$ peak ratios. For pressure-broadened lines, the Lorentzian line-shape function may have a slightly different temperature and pressure dependence for each absorption line due to differing broadening parameters, $\gamma_j^{T_0}$ and $n_j$. Also, spectral line widths are dependent upon gas composition, since broadening parameters are species-specific. However, by choosing identical values of $m$ for each absorption feature near the conditions ($P$, $T$, $\chi_j$) of interest, the $2f$ peak ratios of pressure-broadened lines should be relatively insensitive to differences in the integral in (9) for modest temperature, pressure, and compositional ranges. These effects may be analyzed and simulated by using parameters found in spectral databases such as HITRAN and HITEMP [24, 25]. The most ideal situation, clearly, is to tune the modulation amplitude such that $m$ is near a value of 2.2 so that the integral in (9) is maximized and therefore insensitive to temperature, pressure, and compositional effects for each individual absorption feature.

Since analytical solutions to (9) exist in the literature for Lorentzian line shapes [23, 26], it is possible to derive an expression for pressure-broadened $2f$ peak height ratios provided that the assumption of weak absorption holds. From the work of Arndt [23], the $2f$ peak height for a Lorentzian absorption feature, identified with the subscript $i$, may be written as

$$H_2(\bar{\nu}_{0,i}) \propto S_i pL\frac{2}{m_i^2}\left(2-\frac{2+m_i^2}{\sqrt{1+m_i^2}}\right). \tag{13}$$

Taking the $2f$ peak ratio of two multiplexed lines, identified with subscripts $i = 1$ and 2, yields

$$R = \frac{S_1}{S_2}\left(\frac{2\sqrt{1+m_1^2}-2-m_1^2}{2\sqrt{1+m_2^2}-2-m_2^2}\right)\left(\frac{m_2^2\sqrt{1+m_2^2}}{m_1^2\sqrt{1+m_1^2}}\right). \tag{14}$$

From (14), it is evident that the $2f$ peak ratios are equivalent to line-strength ratios if the modulation indices are equal. This is true for two pure Gaussian line shapes as well, but is not true for two arbitrary Voigt profiles unless they have identical parameters. This can be seen by an inspection of Fig. 2, from which we note that $2f$ peak heights for all Gaussian and Lorentzian line shapes behave identically with $m$, because the line-shape integrals in (9) are identical. However, the behavior of $2f$ peak heights for Voigt line shapes falls anywhere between the two limiting cases shown in Fig. 2. In practice, multiplexed absorption lines that exhibit Voigt line shapes may possess different pressure-broadening coefficients, which will result in a mix of Voigt profiles. Therefore, either a numerical integration of the Voigt line shapes (if accurately known) or a calibration near the measurement conditions allows for a determination of a scaling factor between $2f$ peak ratios and line-strength ratios. In addition, it is often difficult to completely account for differences in laser intensities and lock-in settings, as well as slight differences in $m$, so that a calibration is generally required when performing modulation spectroscopy.

The data in Fig. 2 indicate that the $2f$ peak signal strength varies quite slowly for modulation indices near 2.2. For example, consider the $2f$ peak height for a Lorentzian absorption feature with a temperature coefficient, $n = 0.5$, at 1600 K, modulated with an optimal modulation index of 2.2. First, using (13) or Fig. 2, the range in which the modulation index, $m$, is within 1% of its optimal value at $m \sim 2.2$ is calculated to be $1.90 < m < 2.55$. This range is used, together with (10) and (12), to calculate the corresponding temperature range in which the $2f$ peak intensity of this particular absorption feature varies with temperature precisely as its line strength does to within an error of 1%. For this Lorentzian feature with $n = 0.5$, the temperature range is $1190\,\mathrm{K} < T < 2145\,\mathrm{K}$. For a multiplexed temperature sensor probing two absorption features, this temperature range of nearly 1000 K represents a lower bound, because taking peak ratios tends to mitigate the effects of changes in $m$ with temperature, assuming that both $m$ values are identical and optimal ($m \sim 2.2$). This back-of-the-envelope calculation provides additional assurance that $2f$ peak ratios may be assumed to vary directly with line-strength ratios, for temperature ranges on the order of 1000 K (at combustion temperatures), provided that modulation indices are optimized.

For Gaussian, Lorentzian, or Voigt line shapes, numerical integration of (9) may be performed [27]. In the case of highly broadened and blended line shapes, spectral simulation programs may be used to generate tabular absorbance data, which are readily integrated numerically to simulate $2f$ signal intensities.

## 3 Experimental setup

For the temperature sensor, two fiber-coupled distributed feedback (DFB) diode lasers (10–30 mW), from NEL America Inc., are multiplexed using a $1 \times 2$ single-mode fiber coupler (A.C. Photonics) designed for 1310 nm. The lasers, at 1343 nm and 1392 nm, are placed in ILX Lightwave mounts (LDM-4984) and are driven with an ILX Lightwave modular diode laser controller (LDC-3908) equipped with a 500 mA/9 W current source and temperature-control units (LDC-3916372). The lasers are temperature tuned to lase at wavelengths near the selected absorption features, and are set with a constant bias injection current of about 70 mA. Since the NEL lasers are specified to operate with a maximum current level of 150 mA, the 70-mA current level biases the lasers near the midpoint. An external modulation, consisting of a 1-kHz sawtooth ramp summed with a faster 170-kHz sinusoidal modulation, is fed into each of the current-source units. The two waveforms, with independent amplitude control, are generated using LabVIEW codes running a National Instruments data-acquisition (NI-DAQ) system. The NI-DAQ system consists of a personal computer fitted with a PCI-6115 DAQ board (12-bit A/D conversion) and a BNC-2110 analog I/O block.

The fiber-coupled multiplexed beam is pitched across a test region using a Thorlabs aspheric collimator (F230FC-C). On the catch side, a larger collimator from Oz Optics (HPUCO-25-1300-M-10BQ) is used to focus the free-space beam into a 400-micron-diameter multimode fiber with an numerical aperture (NA) of 0.39 (Thorlabs M20L05). The 400-micron fiber routes the collected signal into a grating-based demultiplexing setup, where a large aspheric lens (Optosigma 023-2392) is used to collimate the output from the 400-micron fiber and send it onto a 25-mm-square diffraction grating with 1200 grooves/mm (Edmund Optics NT43-852). The demultiplexed beams are then sufficiently dispersed in space to be focused with concave mirrors onto individual 10-MHz silicon photodetectors (Thorlabs PDA400). Care is taken to carefully focus and align the separated beams onto the 1-mm-square detector surfaces in order to avoid mode noise distortions caused by the 400-micron fiber. Figure 4 illustrates the experimental setup.

Detector signals from both channels are simultaneously recorded at a 5-MHz sampling rate by the NI-DAQ system using a LabVIEW scope program. $2f$ line shapes are recovered by running a digital lock-in program on LabVIEW with a low-pass filter time constant of 50 kHz. In order to account for wavelength-dependent fluctuations in laser intensity, $I_0$, caused by thermal and mechanical transients, fiber vibrations, and changes in fiber positioning (which affect each laser differently), the value of the $2f$ peak signals at line center are adjusted by dividing them by the corresponding line-center values of $\bar{I}_0$. $\bar{I}_0$ values are calculated by performing polynomial fits to the non-absorbing portions of the laser scans. The line-center value of $\bar{I}_0$ is then simply inferred from the polynomial fit. As mentioned, the $2f$ peak heights, determined using a LabVIEW peak-detector routine, are then divided by the fitted $\bar{I}_0$ value in order to account for laser intensity fluctuations. The peak-detector routine uses an algorithm that fits a quadratic polynomial to sequential groups of data points. Due to the fact that the lock-in low-pass filter smooths the $2f$ line shape, the peak-detector routine does not introduce significant errors into the measurement. Figure 5 is an example of a laser scan with a fit for $\bar{I}_0$ illustrated as well. The corresponding $2f$ line shape for the signal in Fig. 5 is shown in Fig. 6. It is important to note that the error associated with performing polynomial fits to infer $\bar{I}_0$ in our procedure is minimal compared to the error introduced by performing

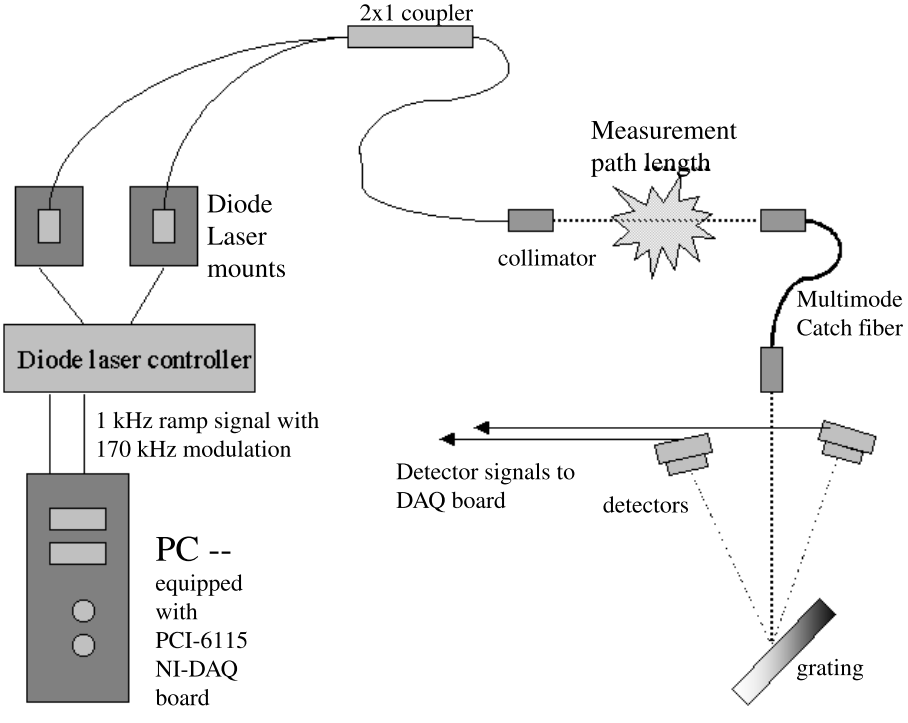


**FIGURE 4** Experimental setup. See text for details

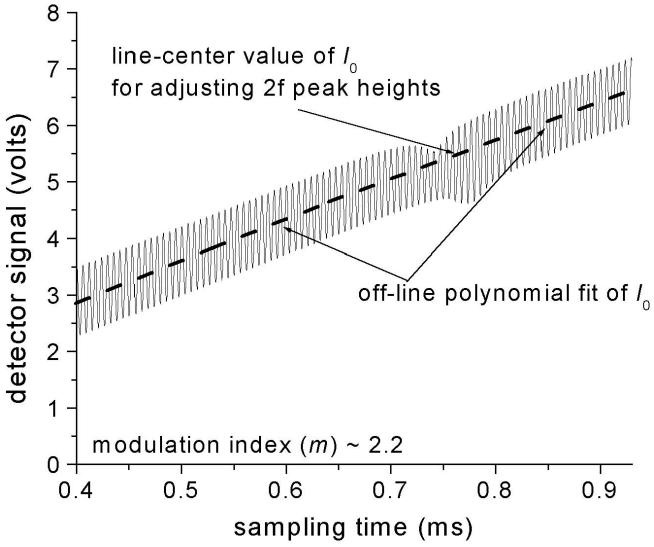


**FIGURE 5** Example of a modulated laser scan. An $I_0$ line fit is depicted, which is used to adjust for laser transmission fluctuations

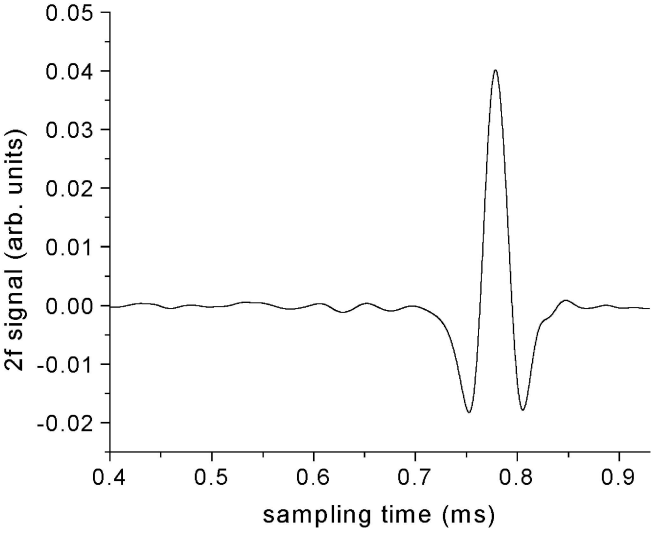


**FIGURE 6** Example $2f$ line shape at 1392 nm. Ambient water vapor at 296 K, 10-cm path length

polynomial fits to determine direct absorption baselines for weakly absorbing features. This is due to a difference in relative measurement scales. A 1% error in $\bar{I}_0$ adds a 1% error to our adjusted $2f$ peak heights. However, for a direct absorption measurement, a 1% error in the baseline fit for a 1% absorption feature (for example) creates a 100% measurement error.

The ability to correct $2f$ peak heights to account for fluctuations in $\bar{I}_0$ is the major advantage of a scanned-wavelength implementation as opposed to a fixed-wavelength method. While fixing the lasers at line center would allow for measurement bandwidths of 50 kHz (the lock-in time constant) as opposed to the scan-rate-limited 1-kHz bandwidth of our present setup, there would be no information on $\bar{I}_0$ since only $I_t$ is measured in (3). The use of free-space optics, in a well-controlled laboratory environment, offers a means to circumvent this problem by using beam splitters to provide $\bar{I}_0$ reference signals prior to the combustion region. In practice, however, it is difficult for reference signals to account for uncertainties and changes in transmission characteristics through a combustor, especially if fiber optic collection is employed. For very low absorbance levels (optically thin), on the order of 1% or less, fixed-wavelength methods may be feasible since $\bar{I}_0$ and $I_t$ are nearly equal. Therefore, only a small error, on the order of the absorbance (1%), is introduced if $I_t$ is assumed to be identical with $\bar{I}_0$. There is much additional literature that recognizes the need for transmission corrections when making WMS measurements [4, 15].

A furnace facility, equipped with a 20 cm path length absorption cell, was used for initial validation experiments of the $2f$ temperature sensor. The tube furnace (Thermolyne F21125) is 40-cm long, of which only the middle 20 cm is occupied by the cell's path length in order to improve temperature uniformity. Temperatures of up to 1100 K are attained with pure water samples (1–15 Torr), ambient air, or water samples diluted with $N_2$. Type K thermocouples are attached to the absorption cell at various mid-span locations to monitor the temperature. Maximum non-uniformity in temperature along the path length is on the order of 25 K. When it is desirable to increase absorbance levels, a double-pass arrangement is used in order to increase the overall absorption path length to 40 cm.

## 4 Results

An example plot of $2f$ peak heights, adjusted to account for laser transmission fluctuations as discussed in the previous section, versus temperatures from 450 K to 1075 K is plotted in Fig. 7 for the absorption feature at 1392 nm. The absorption cell was filled with various amounts of pure water vapor ranging from 1.5 Torr to 2.5 Torr, all of which resulted in peak absorbance levels of less than 10% (satisfying (8)). Three modulation amplitudes were used at each condition near the maximum modulation index: $m \sim 2.2$. Note that with increasing temperature, the value of the modulation amplitude that yields a maximum $2f$ peak height changes slightly. As discussed previously, this is due to an increase in line width, which is predominantly Doppler broadened in this case, as temperature rises. The Doppler half widths of the water va-

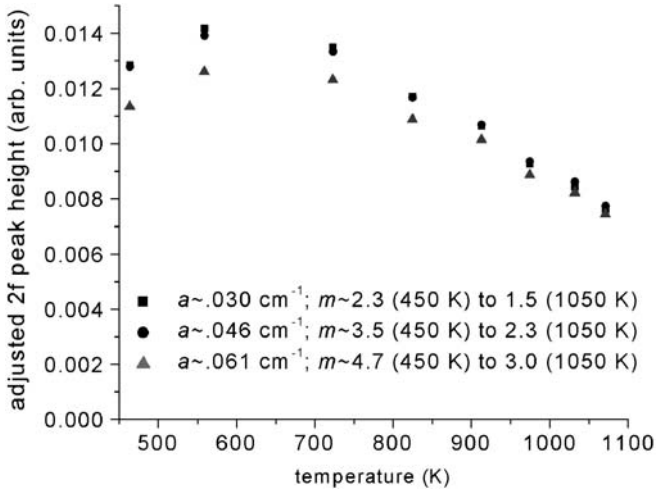


**FIGURE 7** Adjusted $2f$ peak height versus temperature. 1392-nm feature at three modulation depths

por samples increase from 0.013 $cm^{-1}$ to 0.02 $cm^{-1}$ over the measured temperature range, and the collision half widths decrease from 0.0005 to 0.00025 $cm^{-1}$, according to the spectroscopic parameters listed in the HITRAN database [24]. As line width increases, so does the value of modulation amplitude, $a$, needed to achieve the maximum $2f$ signal at $m \sim 2.2$ (see (10) and Fig. 3). As shown in Fig. 7, the modulation depths used in these measurements range from about 0.030 to 0.061 $cm^{-1}$, corresponding to modulation indices, $m$, ranging from approximately 2.3 to 4.7 at 450 K and 1.5 to 3.0 at 1050 K. Note that the general shape of the curve in Fig. 7 reflects the shape of the analogous line strength versus temperature plot shown in Fig. 1. The success of our temperature sensor relies on the fact that these two quantities, the line strength and the $2f$ peak height, are equivalent functions of temperature for appropriate choices of $m$.

Second harmonic peak ratios, at the measurement conditions stated above, are plotted for the 1392-nm and 1343-nm features in Figs. 8 and 9. Figure 8 covers the entire temperature range of the furnace measurements and is normalized such that the largest ratio is unity. Figure 9 covers a smaller temperature span at the higher temperatures, and is again normalized using the largest ratio in the plot. Note that although various modulation depths are used in Fig. 9, corresponding to modulation indices ranging from about 1.5 to 3.5, the use of peak ratios causes the results to collapse onto one curve. This demonstrates one of the simplifying effects of matching the modulation indices for each line. Line strengths and lower-state energies from the HITRAN/HITEMP [24, 25] database are used to calculate line-strength ratios, which are also normalized and plotted in the same figures. Considering the effects of temperature uncertainty and non-uniformity in the cell ($\sim$ 25 K), the data matches the simulated $2f$ ratios (based on line-strength ratio) well. The agreement between $2f$ peak ratios and line-strength behavior, as a function of temperature, demonstrates the additional simplifying effect of optimizing modulation depths.

The need exists to monitor real-time temperature fluctuations in post-combustion flow fields of realistic combustion devices. The temperatures in such flow fields can vary by hundreds of degrees (Kelvin). Figures 8 and 9 clearly demonstrate the potential of a multiplexed $2f$ diode laser sensor for rapidly and accurately monitoring temperatures in gaseous flows (1-kHz bandwidth in this case). For applications in which a fixed-wavelength implementation of $2f$ spectroscopy is feasible, higher measurement bandwidths may be attained, limited only by the lock-in time constant (50 kHz in this case). For fixed-wavelength $2f$ peak height measurements, transmission fluctuations must not exist, or if they do, absorbance levels must be low such that $I_t$ may be assumed to be identical with $\bar{I}_0$. The data in Fig. 9 can be presented in an alternative form to demonstrate the effectiveness of the sensor to infer temperature. In Fig. 10, the data point at 825 K, with $m \sim 2.2$, is used to calibrate the $2f$ sensor. Temperatures at four hotter conditions are extrapolated by using the calibration point and the HITRAN-simulated temperature dependence of the line-strength ratios. The agreement of the $2f$ sensor measurements with the thermocouple measurements is within the

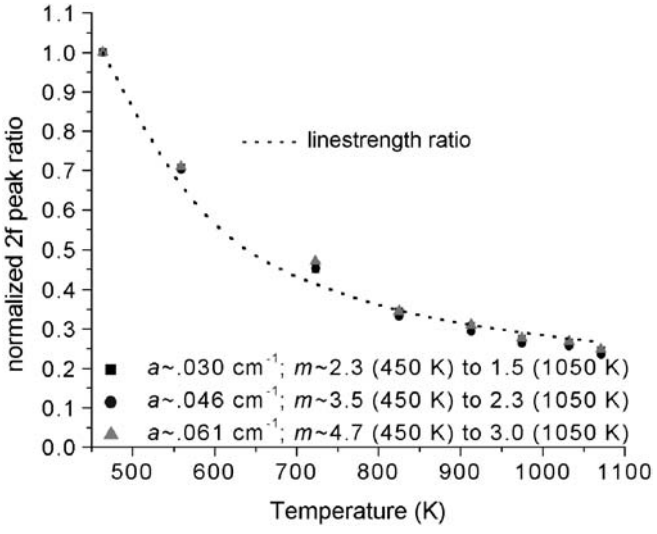


**FIGURE 8** Normalized $2f$ peak ratios versus temperature. 1392-nm signal/1343-nm signal

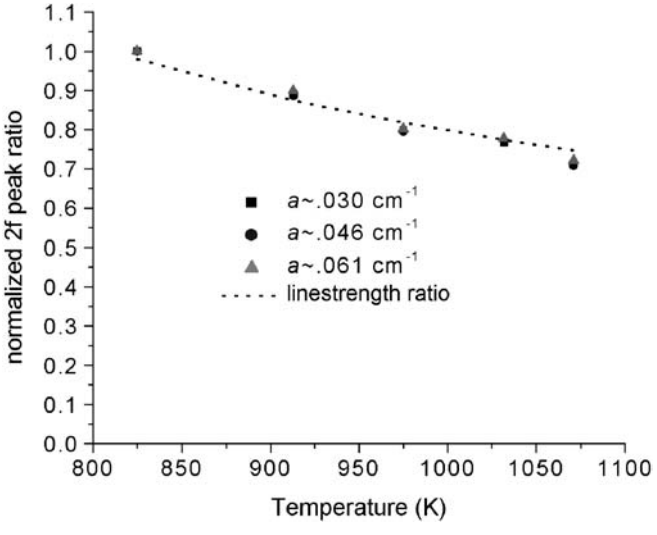


**FIGURE 9** Normalized $2f$ peak ratios versus temperature (reduced temperature range). 1392-nm signal/1343-nm signal

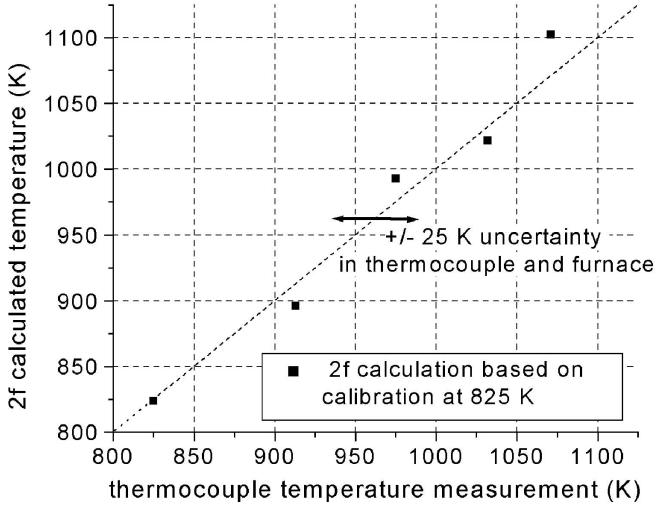


**FIGURE 10** Calibrated $2f$ temperature measurements versus thermocouple measurements (using 1392 nm/1343 nm $2f$ peak ratios). $P = 1.5$–$2.5$ Torr

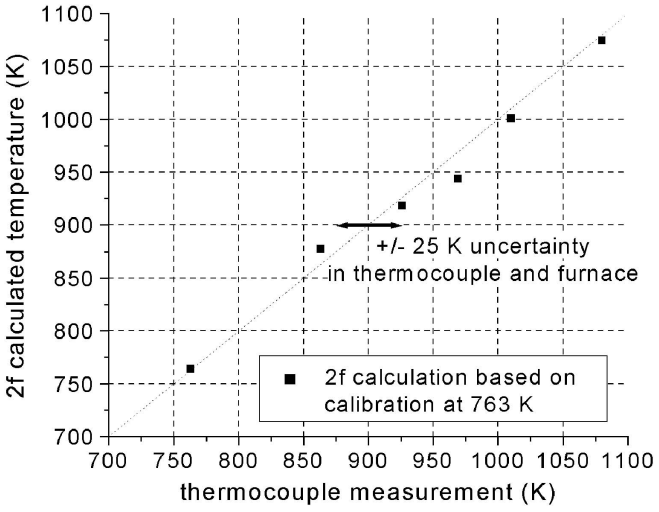


**FIGURE 11** Calibrated $2f$ temperature measurements versus thermocouple measurements (using 1392 nm/1343 nm $2f$ peak ratios). Ambient water vapor, $P = 1$ atm, $m \sim 2.2$

uncertainty and non-uniformity of the thermocouple and furnace ($\pm 25$ K).

A comparison of the SNR of direct absorption measurements with WMS measurements shows a significant improvement of nearly one order of magnitude for $2f$ line shapes ($\sim 0.02\%$ minimum-detectable absorption for a 1-kHz bandwidth). This is consistent with what is found in the literature [14, 28]. Also, there is no ambiguity in the baseline of the $2f$ line shape, which eliminates the baseline-fitting errors common with direct absorption measurements, resulting in more reproducible measurements. This is especially true for weak absorption or if neighboring water lines interfere with the spectral feature and obscure the zero-absorption baseline, which is the case for most lines at higher temperatures and pressures. In certain cases, neighboring features may be broadened and are close enough to lift the baseline trough to a finite absorption level, eliminating the zero-absorption baselines entirely. $2f$ signals are sensitive to line-shape curvature (the second derivative), making them insensitive to baseline. Second-harmonic line shapes are determined by instrument settings and lock-in parameters, which are reproducible and eliminate the need for manual post-processing. The convenience in data processing, along with an improved SNR, gives the $2f$ sensor major advantages for accurate and fast temperature monitoring in many applications.

Finally, in order to generalize our experimental validations to atmospheric pressure situations, identical temperature measurements were carried out on ambient water vapor at atmospheric pressures in the furnace facility. At these conditions, the water absorption features may be modeled as Voigt line shapes that are more heavily pressure broadened than Doppler broadened. Figure 11 shows a temperature measurement analogous to the low-pressure plot of Fig. 10. According to the HITRAN database, collision half widths of the air-broadened ambient water vapor sample are about $0.053\ \mathrm{cm}^{-1}$ and Doppler half widths are about $0.011\ \mathrm{cm}^{-1}$ at the measured conditions. A modulation depth of about $0.14\ \mathrm{cm}^{-1}$ was used for the measurement shown in Fig. 11, corresponding to a modulation index, $m$, near 2.2. The excellent agreement with thermocouple measurements demonstrates the utility of the $2f$ ratio technique for making temperature measurements in a variety of pressure conditions up to atmospheric.

## 5 Conclusions

A comparison of the direct absorption method versus the WMS diagnostic technique is presented in Table 1. While direct absorption measurements have the benefit of enabling absolute measurements of temperature and mole frac-

| Sensing strategy | Benefits | Liabilities |
|---|---|---|
| **Direct absorption** | • Absolute $T$ and $\chi$<br>• No calibration required<br>• Accurate for large absorbance levels<br>• Relatively simple to implement | • Less effective at high $P$ due to lack of zero-absorption baselines<br>• Prone to errors at low absorbance levels due to baseline uncertainties<br>• Insufficient SNR |
| **WMS with second-harmonic detection** | • Derivative method is sensitive to curvature, thereby reducing sensitivity to baseline-fitting errors<br>• Probable benefits at higher pressures due to reduced baseline sensitivity<br>• More accurate and sensitive for small absorbance levels<br>• Improved SNR<br>• Becoming easier to implement with modern software and data-acquisition systems | • Requires a one-point calibration and careful selection of $m$<br>• More complicated for large absorbance levels<br>• More complicated for concentration measurements (additional calibration is required) |

**TABLE 1** A comparison of direct absorption and $2f$ temperature-sensing techniques

tion over large dynamic ranges, they are hampered by low and noisy signal conditions. Accurate and repeatable baseline fits are often not possible to achieve with absorbance levels less than about 10%. The interpretation of $2f$ line shapes, however, is simplified for low absorbance levels under about 10%. This fact, coupled with the SNR improvements afforded by WMS, offers advantageous for many realistic measurement applications.

For the purposes of baseline fitting, spectrally isolated features are desirable for direct absorption measurements. This complicates the use of direct absorption methods for highly pressure-broadened lines, which exist in many realistic combustion devices. In contrast, second-harmonic detection is sensitive to the curvature in absorption lines (the second derivative), making a zero-absorption baseline unnecessary. For highly broadened spectroscopic features, it may not be possible to modulate existing DFB diode lasers with large enough modulation indices to maximize the $2f$ signal and minimize sensitivity in $m$, though new lasers may alleviate this deficiency. As stated earlier, however, $2f$ peak ratios will still vary identically with line-strength ratios provided that $m$ behaves similarly for each absorption feature. At higher pressures exceeding 10 atm, pressure-broadened 'features' are generally composed of overlapping and blended spectroscopic transitions, complicating the selection of an appropriate value of $m$ for each feature. If it is not possible to define a modulation index, due to highly broadened and blended line shapes, temperature measurements would likely rely upon $2f$ simulations based upon accurate high-pressure spectral simulations and calibration experiments performed at the modulation depth, pressure, and temperature conditions of interest.

Wavelength modulation spectroscopy with harmonic detection is becoming easier to implement with the advent of modern data-acquisition and software packages. In addition, it has been shown that the interpretation of $2f$ absorption peak ratios from multiplexed diode lasers is straightforward, provided that modulation indices are optimized, and permits accurate and fast temperature sensing over large temperature ranges in challenging measurement environments. Upcoming tests in realistic combustion flow facilities, and with optimized near-infrared water vapor transitions, aim to demonstrate the merit of this sensing technique for practical diagnostic use, including use at higher temperature and pressure regimes.

**ACKNOWLEDGEMENTS** This work was supported by the Air Force Office of Scientific Research (AFOSR), Aerospace and Materials Science Directorate, with Dr. J. Tishkoff as technical monitor.

## REFERENCES

1 M.G. Allen: Meas. Sci. Technol. **9**, 545 (1998)
2 D.S. Baer, V. Nagali, E.R. Furlong, R.K. Hanson: AIAA J. **34**, 489 (1996)
3 H. Teichert, T. Fernholtz, V. Ebert: Appl. Opt. **42**, 2043 (2003)
4 J.A. Silver, D.J. Kane: Meas. Sci. Technol. **10**, 845 (1999)
5 D. Richter, D.G. Lancaster, F.K. Tittel: Appl. Opt. **39**, 4444 (2000)
6 S.I. Chou, D.S. Baer, R.K. Hanson, W.Z. Collison, T.Q. Ni: J. Vac. Sci. Technol. B **19**, 477 (2001)
7 D.C. Hovde, J.T. Hodges, G.E. Scace, J.A. Silver: Appl. Opt. **40**, 829 (2001)
8 L.C. Philippe, R.K. Hanson: Opt. Lett. **16**, 2002 (1992)
9 S.T. Sanders, J.A. Baldwin, T.P. Jenkins, D.S. Baer, R.K. Hanson: Proc. Combust. Inst. **28**, 587 (2000)
10 V. Nagali, R.K. Hanson: Appl. Opt. **36**, 9518 (1997)
11 M.P. Arroyo, R.K. Hanson: Appl. Opt. **32**, 6104 (1993)
12 E.R. Furlong: Diode-laser Absorption Spectroscopy Applied for the Active Control of Combustion. Ph.D. dissertation, Department of Mechanical Engineering, Stanford University, Stanford, CA, 1998
13 V. Nagali, S.I. Chou, D.S. Baer, R.K. Hanson: J. Quantum Spectrosc. Radiat. Transfer **57**, 795 (1997)
14 D.S. Bomse, A.S. Stanton, J.A. Silver: Appl. Opt. **31**, 718 (1992)
15 T. Fernholtz, H. Teichert, V. Ebert: Appl. Phys. B **75**, 229 (2002)
16 T. Aizawa: Appl. Opt. **40**, 4894 (2001)
17 J.J. Nikkari, J.M. Di Iorio, M.J. Thomson: Appl. Opt. **41**, 446 (2002)
18 T.P. Jenkins, P.A. DeBarber, M. Oljaca: A Rugged Low-cost Diode Laser Sensor for $H_2O$ and Temperature Applied to a Spray Flame. Presented at: 41st Aerospace Sciences Meet. Exhib., American Institute of Aeronautics and Astronautics, Reno, NV, 6–9 January (2003)
19 J.M. Supplee, E.A. Whittaker, W. Lenth: Appl. Opt. **33**, 6294 (1994)
20 J. Reid, D. Labrie: Appl. Phys. B **26**, 203 (1981)
21 L.C. Philippe, R.K. Hanson: Appl. Opt. **32**, 6090 (1993)
22 P. Kluczynski, O. Axner: Appl. Opt. **38**, 5803 (1999)
23 R. Arndt: J. Appl. Phys. **36**, 2522 (1965)
24 L.S. Rothman, A. Barbe, D.C. Benner, L.R. Brown, C. Camy-Peyret, M.R. Carleer, K. Chance, C. Clerbaux, V. Dana, V.M. Devi, A. Fayt, J.-M. Flaud, R.R. Gamache, A. Goldman, D. Jacquemart, K.W. Jucks, W.J. Lafferty, J.-Y. Mandin, S.T. Massie, V. Nemtchinov, D.A. Newnham, A. Perrin, C.P. Rinsland, J. Schroeder, K.M. Smith, M.A.H. Smith, K. Tang, R.A. Toth, J. Vander Auwera, P. Varanasi, K. Yoshino: J. Quant. Spectrosc. Radiat. Transfer **82**, 5 (2003)
25 http://cfa-www.harvard.edu/hitran/
26 H. Wahlquist: J. Chem. Phys. **35**, 1708 (1961)
27 G.V.H. Wilson: J. Appl. Phys. **34**, 3276 (1963)
28 D.C. Hovde, C.A. Parsons: Appl. Opt. **36**, 1135 (1997)